Figure S1

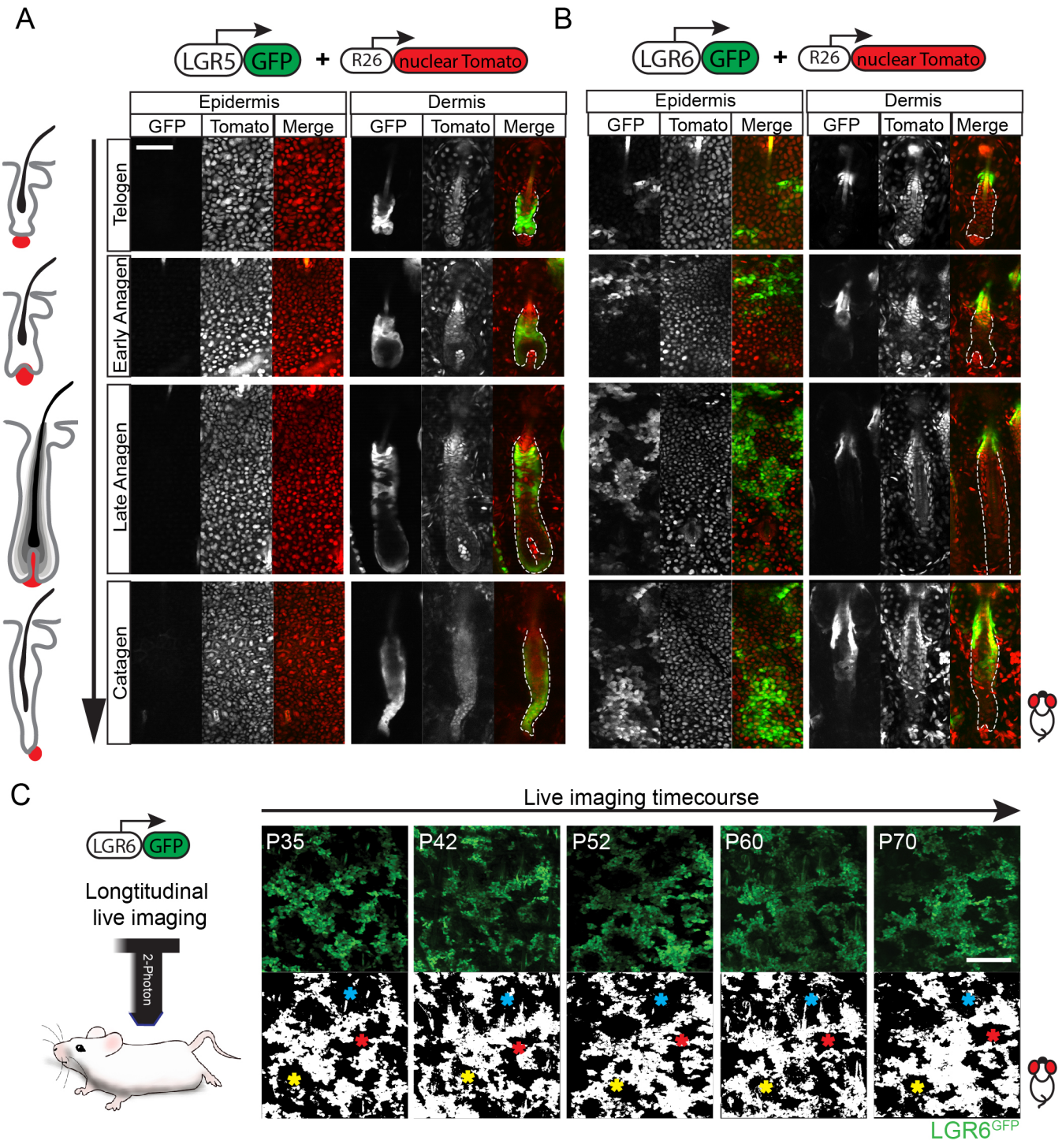
A
LGR5 GFP + R26 nuclear Tomato
Epidermis
Dermis
GFP
Tomato
Merge
Telogen
Early Anagen
Late Anagen
Catagen
B
LGR6 GFP + R26 nuclear Tomato
C
LGR6 GFP
Longtitudinal live imaging
2-Photon
Live imaging timecourse
P35
P42
P52
P60
P70
LGR6GFP

Figure S1. Localization and dynamics of Lgr5 and Lgr6-expressing stem cells in the mouse skin. Related to Figure 1. (A-B) Representative images from serial optical sectioning of the live mouse skin, at timepoints corresponding to the different stages of the hair cycle, acquired by two-photon microscopy. Optical planes that correspond to the basal layer of the epidermis and hair follicle containing dermis, are shown. GFP signal marks cells that express Lgr5 (A) or Lgr6 (B), respectively. A ubiquitous red fluorescent *in vivo* reporter was used as a nuclear counterstain to distinguish the different tissue compartments. Note the distinct clusters of epidermal stem cells expressing Lgr6. White dashed line shows the margins of individual hair follicles. (C) Live imaging time course of $Lgr6^{GFP}$ stem cells in the interfollicular epidermis. Top panel shows the localization of $Lgr6^{GFP}$ stem cells during 35 days of imaging. Individual frames are single optical sections at the plane which corresponds to the basal layer of the epidermis from the same location of the skin. Bottom panel shows a threshold analysis of the GFP signal to illustrate the territories of $Lgr6^{GFP}$ stem cells, which remain largely unchanged over time. Asterisks mark the exact corresponding locations across the different time points. Scale bar: 50μm (A-B), 200μm (C).

Figure S2

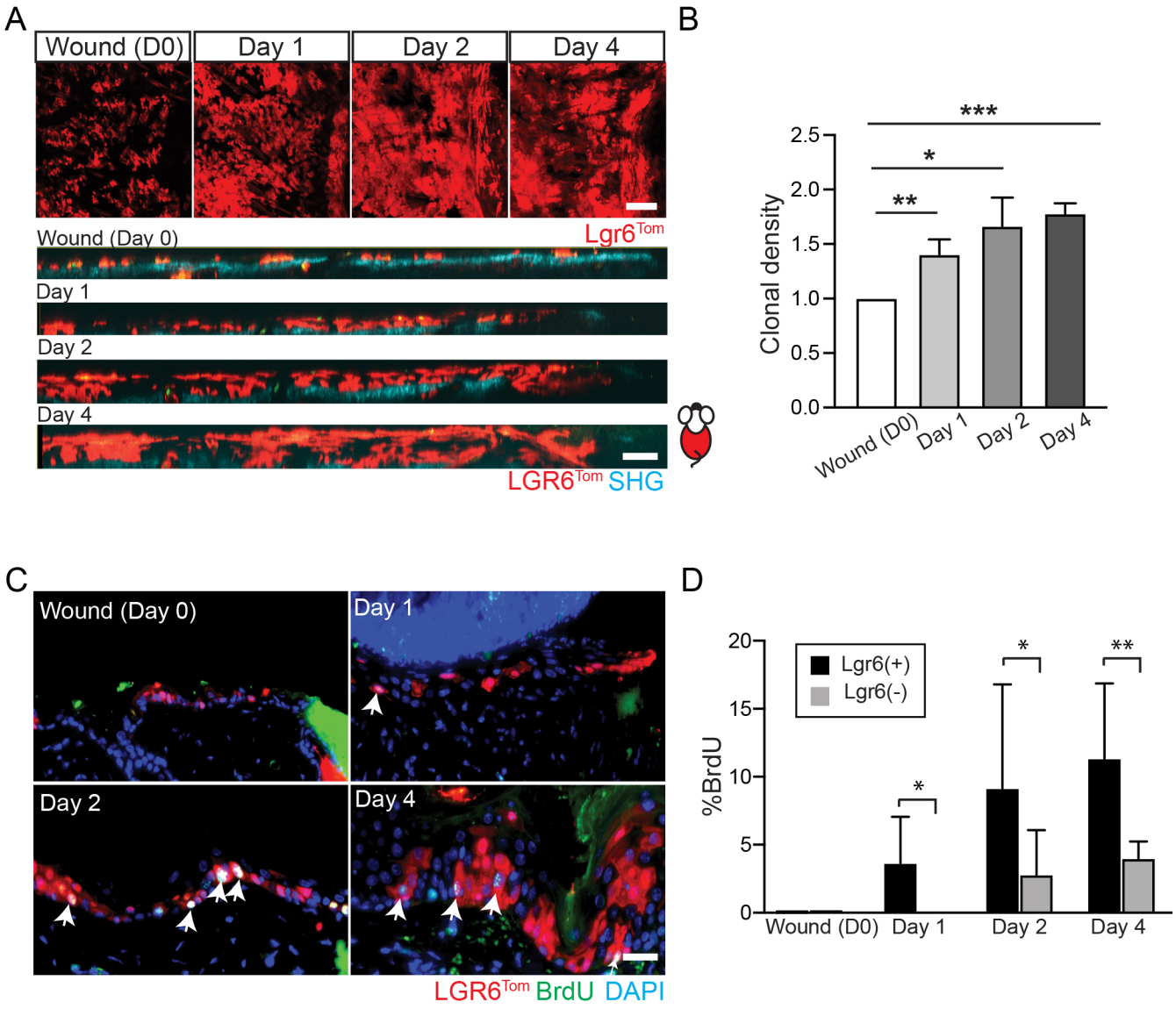
A
Wound (D0)
Day 1
Day 2
Day 4
Wound (Day 0)
Lgr6Tom
Day 1
Day 2
Day 4
LGR6Tom SHG
B
Clonal density
2.5
2.0
1.5
1.0
0.5
0.0
***
*
**
Wound (D0)
Day 1
Day 2
Day 4
C
Wound (Day 0)
Day 1
Day 2
Day 4
LGR6Tom BrdU DAPI
D
%BrdU
20
15
10
5
0
Lgr6(+)
Lgr6(-)
*
*
**
Wound (D0)
Day 1
Day 2
Day 4

Figure S2. Lineage tracing of Lgr6 stem cells during wound re-epithelialization. Related to Figure 1. (A) Representative top-down and side views of the epidermis at the wound edge, taken at the indicated time intervals. Lgr6 stem cells were marked with the Tomato Cre reporter ($Lgr6^{Tom}$) prior to wounding and traced during the first four days of wound re-epithelialization. (B) Quantification of the $Lgr6^{Tom}$ population growth at the wound edge. N = 3 mice re-imaged at indicated timepoints, (Day 1) p = 0.0069; (Day 2) p = 0.0116; (Day 3) p = 0.0001. (C) Representative tissue sections of the wound edge, taken at the indicated time points. Mice were treated with BrdU two hours before the tissue was harvested. White arrows show $Lgr6^{Tom}$ stem cells that have incorporated BrdU, indicating active proliferation. (D) Quantification of the proliferative activity of $Lgr6^{Tom(+)}$ and $Lgr6^{Tom(-)}$ stem cells during wound re-epithelialization, based on the relative BrdU incorporation. (Day 1) n = 5, p = 0.0431; (Day 2) n = 8, p = 0.0486; (Day 4) n = 8, p = 0.0026. Scale bars: 50μm (A), 20μm (C).

Figure S3

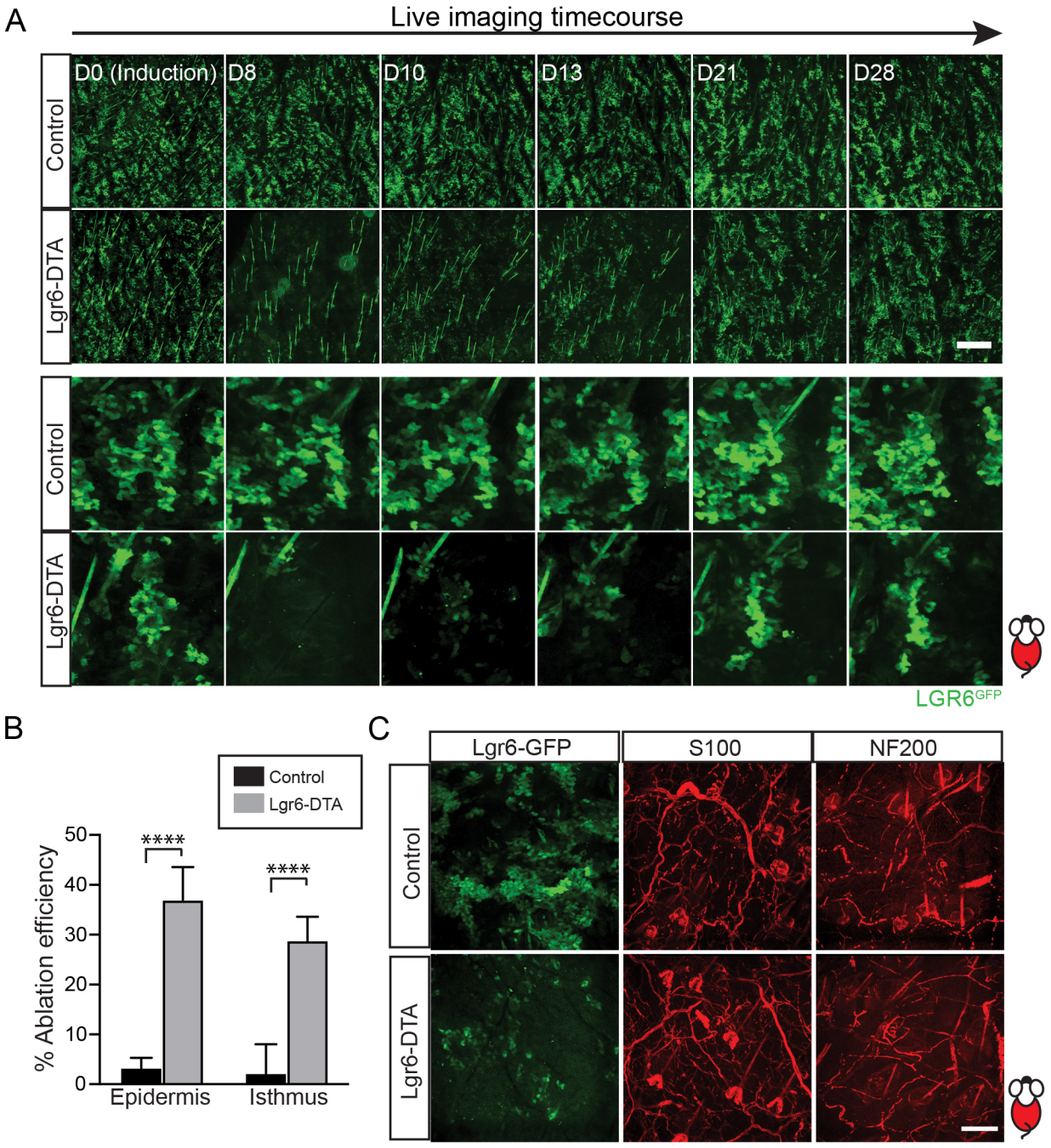
A
Live imaging timecourse
D0 (Induction)
D8
D10
D13
D21
D28
Control
Lgr6-DTA
Control
Lgr6-DTA
LGR6GFP
B
Control
Lgr6-DTA
% Ablation efficiency
50
40
30
20
10
0
****
****
Epidermis
Isthmus
C
Lgr6-GFP
S100
NF200
Control
Lgr6-DTA

Figure S3. Dynamics of diphtheria toxin-mediated ablation and recovery of Lgr6 stem cells. Related to Figure 2. (A) Live imaging time course of $Lgr6^{GFP}$ stem cells in the interfollicular epidermis of control and Lgr6-DTA mice. Individual panels show a low (top rows) and high (bottom rows) magnification views of the same areas of the epidermis imaged at the indicated timepoints. Note the reduction of GFP signal during the first two weeks following DTA induction, indicating effective ablation of $Lgr6^{GFP}$ stem cells. After 21 days, newly specified $Lgr6^{GFP}$ are found occupying the same niches within the epidermis. (B) Quantification of cell ablation efficiency based on TUNEL analysis. In the IFE, $n = 12$ (control) and 6 (Lgr6-DTA), $p < 0.0001$; in the isthmus, $n = 7$ (control) and 6 (Lgr6-DTA), $p < 0.0001$. (C) Whole-mount immunostaining of skin biopsies harvested at 10 days after DTA induction. Note that the ablation of $Lgr6^{GFP}$ stem cells does not affect the density or organization of the nerves. Panel A (top rows) shows tiled images of the mouse skin constructed from multiple fields-of-view. Scale bar: 200μm (A-B), 100μm (C).

Figure S4

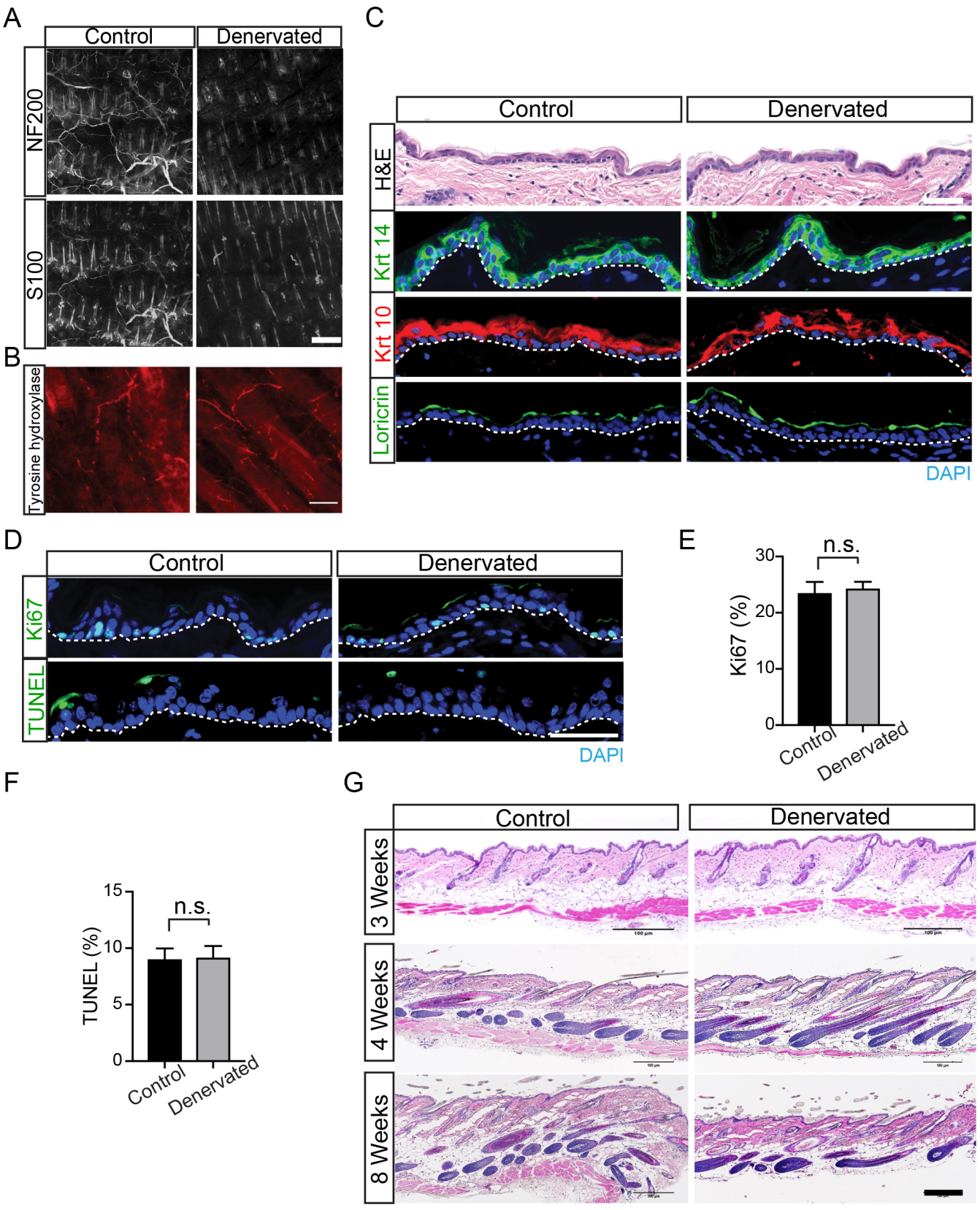
A
Control
Denervated
NF200
S100
B
Tyrosine hydroxylase
C
Control
Denervated
H&E
Krt 14
Krt 10
Loricrin
DAPI
D
Control
Denervated
Ki67
TUNEL
DAPI
E
n.s.
Ki67 (%)
30
20
10
0
Control
Denervated
F
n.s.
TUNEL (%)
15
10
5
0
Control
Denervated
G
Control
Denervated
3 Weeks
4 Weeks
8 Weeks

Figure S4. Denervation does not affect homeostasis of the interfollicular epidermis or hair cycling. Related to Figure 4. (A) Whole-mount immunostaining for S100 and NF200 of biopsies harvested from the intact or denervated side of the back skin one month after denervation surgery shows the absence of sensory nerves in the denervated side of the back skin. (B) Tyrosine hydroxylase immunostaining shows sympathetic nerves are still present after transection of the dorsal roots. (C) Hematoxylin and eosin (H&E) staining and immunofluorescence staining of skin sections show no significant differences in morphology or tissue organization between control and denervated skin. (D) Cell proliferation (Ki67) and apoptosis (TUNEL) analysis of skin sections from control or denervated back skin. (E) Quantification of cell proliferation based on Ki67 staining; n = 82 analyzed samples from 4 mice, p = 0.49. (F) Quantification of cell death based on TUNEL staining; n = 54 analyzed samples from 3 mice, p = 0.8552. (G) H&E staining showing no apparent differences in hair growth between normal and denervated skin. Panel A shows tiled images of the mouse skin constructed from multiple fields-of-view. Scale bars: 100μm (A, G), 50μm (B), 20μm (C, D).

Figure S5

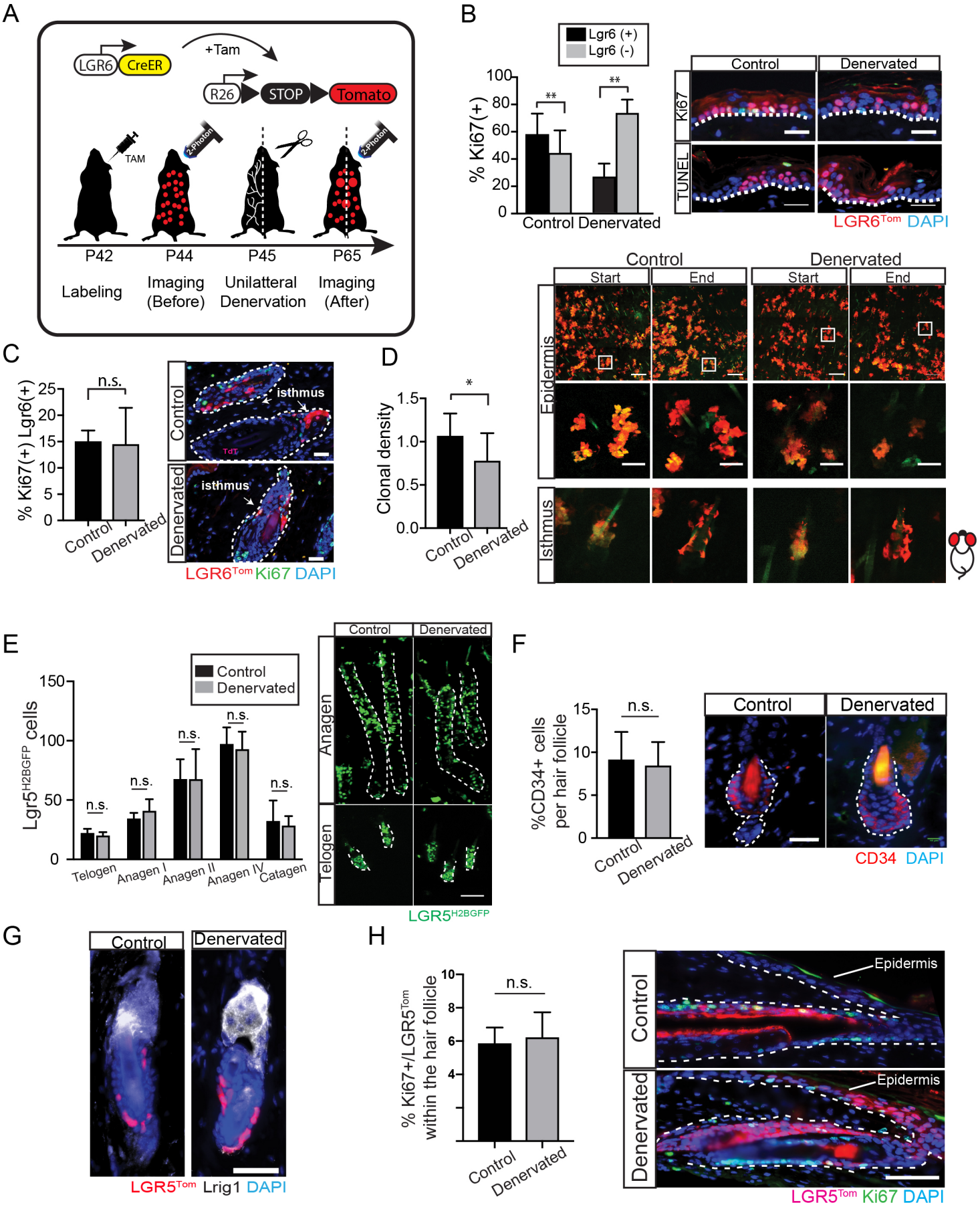
A
LGR6
CreER
+Tam
R26
STOP
Tomato
TAM
2-Photon
P42
P44
P45
P65
Labeling
Imaging (Before)
Unilatteral Denervation
Imaging (After)
B
Lgr6 (+)
Lgr6 (-)
% Ki67(+)
Control
Denervated
Ki67
TUNEL
LGR6Tom DAPI
C
% Ki67(+) Lgr6(+)
n.s.
isthmus
TdT
LGR6Tom Ki67 DAPI
D
Clonal density
*
Start
End
Epidermis
Isthmus
E
Lgr5H2BGFP cells
Telogen
Anagen I
Anagen II
Anagen IV
Catagen
Anagen
LGR5H2BGFP
F
%CD34+ cells per hair follicle
CD34 DAPI
G
LGR5Tom Lrig1 DAPI
H
% Ki67+/LGR5Tom within the hair follicle
Epidermis
LGR5Tom Ki67 DAPI

Figure S5. Analysis of stem cell dynamics after skin denervation. Related to Figure 4. (A) Schematic of experimental design for lineage tracing $Lgr6^{Tom}$ stem cells in the normal (control) and denervated side of back skin by live imaging. (B) Immunofluorescence of interfollicular epidermis samples shows cell proliferation (Ki67) or cell death (TUNEL). Quantification of cell proliferation of epidermal stem cells in intact (control) versus denervated back skin; n = 1048 $Lgr6^{Tom(+)}$ cells (p = 0.0084), n = 1469 cells $Lgr6^{Tom(-)}$ cells (p = 0.0036), from 5 mice. (C) Quantification of cell proliferation of Lgr6Tom stem cells in the hair follicle isthmus; n = 383 cells from 4 mice, p = 0.88. Immunofluorescence shows cell proliferation (Ki67) within the $Lgr6^{Tom}$ stem cell population in the hair follicle isthmus. White dashed line demarcates the margins of hair follicles. (D) Quantification of clonal density measured as the fraction of $Lgr6^{Tom}$ clones in the epidermis at the end of the tracing period; n = 6, p = 0.0128. Representative examples of low and high magnification images of the same areas of the back skin that were imaged at the beginning and end of the tracing period, illustrating the clonal behavior of $Lgr6^{Tom}$ stem cells. (E) Single cell lineage tracing of hair follicle stem cells by longitudinal live imaging. Graph shows the quantification of $Lgr5^{H2BGFP}$ stem cells at different stages of the hair cycle in control and denervated skin. Telogen: n = 12, p = 0.2586; Anagen I: n = 8, P = 0.2697; Anagen II: n = 22, P = 0.9921; Anagen III: n = 16, p = 0.5381; Catagen: n = 21, p = 0.4971; see also Fig. 5C for details on the genetic alleles used for this experiment. (F) Analysis of CD34+ hair follicle stem cells in denervated dorsal skin compared with control. Quantification of CD34+ stem cells was performed by flow cytometry; n = 15 mice, p = 0.052. (G) Immunofluorescence analysis of skin sections shows the location of $Lgr5^{Tom}$ hair follicle stem cells relative to the Lrig1-expressing cells in the isthmus. (H) Quantification of cell proliferation (Ki67 staining) of $Lgr5^{Tom}$ hair follicle stem cells after wounding; n = 3 mice, p = 0.7386. Representative images showing proliferation in $Lgr5^{Tom}$ cells after wounding. White dashed line demarcates the border between epidermis, hair follicle and dermis. Scale bars: 50 μm Panel A (left column) shows tiled images of the mouse skin constructed from multiple fields-of-view. Scale bars: 20 μm (B, C, F), 50 μm (D, E, G, H).

Figure S6

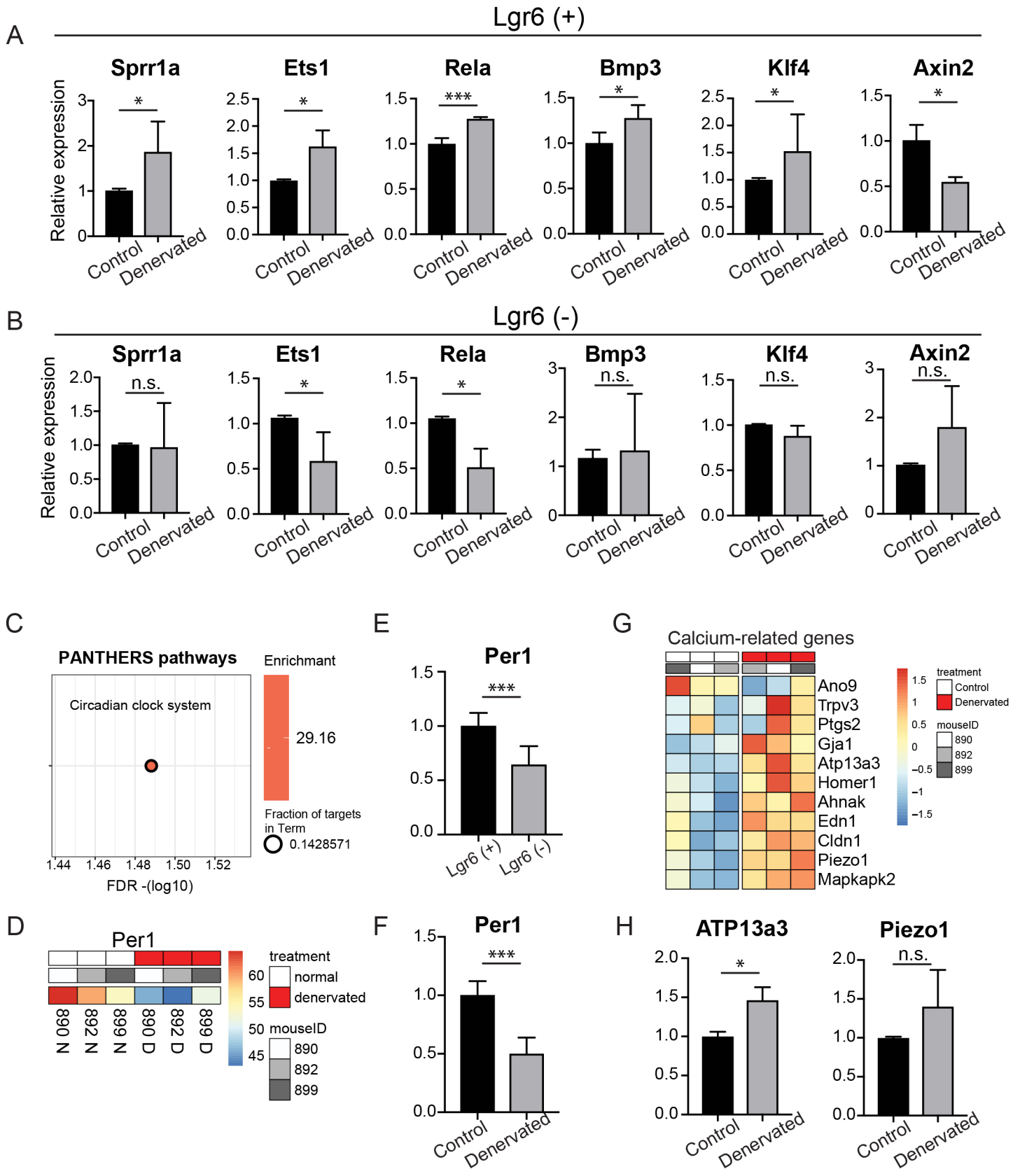
A
Lgr6 (+)
Sprr1a
Ets1
Rela
Bmp3
Klf4
Axin2
Relative expression
Control
Denervated
B
Lgr6 (-)
n.s.
C
PANTHERS pathways
Enrichmant
Circadian clock system
29.16
Fraction of targets in Term
0.1428571
FDR -(log10)
D
Per1
treatment
normal
denervated
mouseID
890
892
899
E
Per1
Lgr6 (+)
Lgr6 (-)
F
Per1
G
Calcium-related genes
Ano9
Trpv3
Ptgs2
Gja1
Atp13a3
Homer1
Ahnak
Edn1
Cldn1
Piezo1
Mapkapk2
H
ATP13a3
Piezo1

Figure S6. Gene expression analysis of Lgr6(+) and Lgr6(-) cells from normal or denervated back skin. Related to Figure 6. (A-B) qRT-PCR analysis of representative genes involved in stem cell regulation. Unpaired t-test analysis, (A) *Sprr1a*: n = 4, p = 0.0459; *Ets1*: n = 3, p = 0.0213; *Rela*: n = 4, p = 0.0008; *BMP3*: n = 3, p = 0.0111; *Klf4*: n = 6; p = 0.0314; *Axin2*: n = 3, p = 0.0107; (B) *Sprr1a*: n = 3, p = 0.9198; *Ets1*: n = 3, p = 0.0804; *Rela*: n = 3, p = 0.0104; *BMP3*: n = 3, p = 0.8308; *Klf4*: n = 3, p = 0.1225; *Axin2*: n = 3, p = 0.2248; (C) PANTHER pathway analysis shows an enrichment in the circadian clock system, downregulated in $Lgr6^{Tom}$ cells isolated from denervated skin. (D) Heatmap showing expression of circadian clock gene *Per1* in normal and denervated skin. (E) qRT-PCR analysis of *Per1* expression in Lgr6(+) versus Lgr6(-) epidermal stem cells; unpaired t-test, n = 7, p = 0.0002. (F) qRT-PCR analysis of *Per1* expression in $Lgr6^{Tom}$ cells isolated from denervated skin versus control, n = 7, $p < 0.001$. (G) Heatmap shows expression of genes involved in calcium signaling in normal and denervated skin. (H) qRT-PCR analysis of two representative calcium-related genes, *ATP13a3* and *Piezo1*, which are differentially expressed in epidermal $Lgr6^{Tom}$ stem cells between the denervated and normal side of the mouse back skin. Unpaired t-test, *ATP13a3*: n = 3, p = 0.0097; *Piezo1*: n = 3, p = 0.2102.

Table S1. Primer sequences for *qRT-PCR* analysis. Related to STAR Methods.

Gene	Forward (5'-3')	Reverse (5'-3')
Sprr1a	CAGAGAACCTGCTCTTCTCTGAGT	GTGGCAGGGATCCTTGGTTT
Ets1	AAACCATATCAGGTTAATGGA	ATGAAGCTGGGCTCTGAGAA
Rela	ACAGATACCACCAAGACACA	TGTGGATGAGGCCGGTGAGGT
Bmp3	TTCTGCCTGAACCTGGCACA	AGCATATGCTCCGACACCTT
Klf4	AGTCTGACATGGCTGTCAGCG	AGTGGGGGAAGTCGCTTCAT
Axin2	ACTGACCGACGATTCCATGT	CTGCGATGCATCTCTCTCTG
Per1	ACCAGGTCATTAAGTGTGTGC	CTCTCCCGGTCTTGCTTCA
ATP13a3	TGGGTGATGGGGCTGGGCTGA	AAGATCCTAGGGTGCTTCTGT
Piezo1	GACGCTGGTCATTGTGTTGCTG	GTCAAGGTCAGGTTCCGTGGTC
GAPDH	AACGGGAAGCCCATCACCATCTT	CAGCCTTGGCAGCACCAGTGG